CrossMark

Eddington-limited Accretion in $z \sim 2$ *WISE*-selected Hot, Dust-obscured Galaxies

Jingwen Wu[1,2], Hyunsung D. Jun[3,4], Roberto J. Assef[5], Chao-Wei Tsai[2], Edward L. Wright[2], Peter R. M. Eisenhardt[3], Andrew Blain[6], Daniel Stern[3], Tanio Díaz-Santos[5], Kelly D. Denney[7,8], Brian T. Hayden[9,10], Saul Perlmutter[9,10], Greg Aldering[9], Kyle Boone[9,10], and Parker Fagrelius[9,10]

[1] National Astronomical Observatories, Chinese Academy of Sciences, 20A Datun Road, Chaoyang District, Beijing, 100012, People's Republic of China; jingwen@nao.cas.cn

[2] Department of Physics and Astronomy, University of California, Los Angeles, CA 90095, USA

[3] Jet Propulsion Laboratory, California Institute of Technology, 4800 Oak Grove Drive, Pasadena, CA 91109, USA

[4] School of Physics, Korea Institute for Advanced Study, 85 Hoegiro, Dongdaemun-gu, Seoul 02455, Republic of Korea

[5] Universidad Diego Portales, Av Republica 180, Santiago, Región Metropolitana, Chile

[6] Department of Physics and Astronomy, University of Leicester, LE1 7RH Leicester, UK

[7] Department of Astronomy, The Ohio State University, 140 West 18th Avenue, Columbus, OH 43210, USA

[8] Illumination Works, LLC, 5550 Blazer Parkway, Dublin, OH, 43017, USA

[9] E.O. Lawrence Berkeley National Lab, 1 Cyclotron Road, Berkeley, CA, 94720, USA

[10] Department of Physics, University of California Berkeley, Berkeley, CA, 94720, USA

Abstract

Hot, dust-obscured galaxies, or "Hot DOGs," are a rare, dusty, hyperluminous galaxy population discovered by the *WISE* mission. Predominantly at redshifts 2–3, they include the most luminous known galaxies in the universe. Their high luminosities likely come from accretion onto highly obscured supermassive black holes (SMBHs). We have conducted a pilot survey to measure the SMBH masses of five $z \sim 2$ Hot DOGs via broad Hα emission lines, using Keck/MOSFIRE and Gemini/FLAMINGOS-2. We detect broad Hα emission in all five Hot DOGs. We find substantial corresponding SMBH masses for these Hot DOGs ($\sim 10^9 \, M_\odot$), and their derived Eddington ratios are close to unity. These $z \sim 2$ Hot DOGs are the most luminous active galactic nuclei for their BH masses, suggesting that they are accreting at the maximum rates for their BHs. A similar property is found for known $z \sim 6$ quasars. Our results are consistent with scenarios in which Hot DOGs represent a transitional, high-accretion phase between obscured and unobscured quasars. Hot DOGs may mark a special evolutionary stage before the red quasar and optical quasar phases, and they may be present at other cosmic epochs.

Key words: galaxies: evolution – galaxies: high-redshift – galaxies: ISM – infrared: galaxies – quasars: supermassive black holes

1. Introduction

Gravitational accretion onto supermassive black holes (SMBHs) is one of the major energy production sources in galaxies, powering active galactic nuclei (AGNs). Its scale and intensity (generally described as the quasar luminosity normalized by the Eddington luminosity, linearly proportional to the mass of the BH, i.e., the "Eddington ratio") are thought to be the most important parameters for governing AGN properties (e.g., Trump et al. 2011; Shen & Ho 2014). High Eddington ratios (as well as super-Eddington accretion) have only been reported in a small fraction of unobscured quasars (e.g., Shen et al. 2008, 2011; Jun & Im 2013). The average Eddington ratio for all Sloan Digital Sky Survey (SDSS) quasars is 0.26 ± 0.34 (Shen et al. 2011). Systematically higher Eddington ratios, slightly above unity, have been reported for SMBHs in quasars at very high redshifts ($z \sim 6$ and above; Fan et al. 2006; Willott et al. 2010; De Rosa et al. 2011), while in the local universe, ultraluminous X-ray sources (ULXs) are believed to often be hosted by stellar-mass compact objects accreting significantly above the Eddington limit. Notably, X-ray pulsations have been detected for three ULXs, implying that the compact objects in those systems are neutron stars (Bachetti et al. 2014; Fürst et al. 2016; Israel et al. 2017b), with an inferred peak isotropic luminosity of ~ 1000 times the Eddington limit in at least one system (Israel et al. 2017a). Despite its importance, the observed Eddington-limited accretion in $z = 6$–7 quasars remains poorly understood. It may be the key to understanding

the formation and coevolution of the first generation of SMBHs and their host galaxies and to explaining how a few to 10 billion solar-mass SMBHs were able to build up their masses when the universe was only ~ 1 Gyr old (e.g., Wu et al. 2015).

Explanations for the coevolution of SMBHs and their hosts often focus on galaxy merging (e.g., Hopkins et al. 2006, 2008; Somerville et al. 2008). In these scenarios, major mergers trigger a starburst at their coalescing center and feed SMBHs, whose growth and feedback will eventually sweep out gas and dust, terminating star formation and leaving a visible quasar with fading luminosity. During these processes, highly obscured, highly luminous phases accompanied by highly accreting SMBHs are expected. These models predict an important phase where galaxies are highly obscured yet exceedingly luminous.

High-luminosity, infrared-dominant galaxies were first discovered by Kleinmann & Low (1970) and Rieke & Low (1972). Significant populations of such galaxies were found by the *Infrared Astronomical Satellite* (*IRAS*; Neugebauer et al. 1984) in the local universe and then extended to the more distant universe (especially to the most rapid evolution epoch at $z = 2$–3) by later infrared space missions and ground-based submillimeter facilities. Milestones include the discovery of the submillimeter galaxies (SMGs; see Blain et al. 2002 and Casey et al. 2014, for a review) in 850 μm and 1 mm surveys and the discovery of dust-obscured galaxies (DOGs; Dey et al. 2008) by *Spitzer* 24 μm surveys (e.g., Rigby et al. 2004;

Donley et al. 2007; Yan et al. 2007; Farrah et al. 2008; Lonsdale et al. 2009). Both populations are at $z \sim 2$ (Chapman et al. 2005; Dey et al. 2008). In general, SMGs are thought to be at an earlier phase of the merger/AGN evolution, when the starburst still dominates the luminosity, while in the DOG phase a hidden AGN becomes increasingly influential, representing a transitional stage when the AGN contribution overtakes star formation and becomes the dominant energy source (Dey et al. 2008; Bussmann et al. 2009; Narayanan et al. 2010). More recently, surveys with the *Herschel Space Telescope* (Pilbratt et al. 2010), as well as the South Pole Telescope (Carlstrom et al. 2011) and the Atacama Cosmology Telescope (Swetz et al. 2011), have extended the area surveyed at submillimeter wavelengths to hundreds of square degrees, highlighting dusty star-forming galaxies to even higher redshifts (e.g., Riechers et al. 2013; Dowell et al. 2014), although a large fraction of the most luminous galaxies are lensed (e.g., Negrello et al. 2010; Vieira et al. 2013; Bussmann et al. 2015). The *WISE* mission (Wright et al. 2010) enabled all-sky selection of dusty, infrared galaxies and is more efficient in selecting red quasars than previous surveys (e.g., Glikman et al. 2007), either by *WISE* colors alone (e.g., Stern et al. 2012; Assef et al. 2013) or combined with other UV to near-IR surveys (e.g., Banerji et al. 2013, 2015; Hainline et al. 2014).

Benefiting from its all-sky coverage, *WISE* is able to identify the most extreme, dusty, highly obscured AGNs in the universe. One of the most successful examples is the discovery of the hyperluminous, hot, dust-obscured galaxies (Hot DOGs; Eisenhardt et al. 2012; Wu et al. 2012). These galaxies were selected by looking for objects strongly detected by *WISE* at 12 and/or 22 μm, but only faintly or not at all at 3.4 and 4.6 μm, i.e., "W1W2-dropout" galaxies (Eisenhardt et al. 2012). The selected galaxies lie between redshifts 1.5 and 4.6, their distribution peaking at $z = 2$–3 (Eisenhardt et al. 2012; Assef et al. 2015). Their luminosities are high (Wu et al. 2012; Bridge et al. 2013; Jones et al. 2014; Assef et al. 2015; Tsai et al. 2015; Fan et al. 2016a; Farrah et al. 2017), mostly well above $10^{13} L_{\odot}$, and they do not show evidence of lensing (Wu et al. 2014; Tsai et al. 2015). The most luminous 10% even exceed $10^{14} L_{\odot}$, comparable to the most luminous quasars known (Assef et al. 2015), and include the single most luminous galaxy or quasar on record so far, the Hot DOG WISE J2246-0526 at $z = 4.593$ (Tsai et al. 2015; Díaz-Santos et al. 2016). This discovery achieved one of the primary *WISE* science goals: finding the most luminous galaxies in the universe.

Having a consistent spectral energy distribution (SED) shape (Wu et al. 2012; Tsai et al. 2015; C. Tsai et al. 2017, in preparation), which is characterized by an unusually high mid-IR to submillimeter ratio, Hot DOGs are quite different from most other well-studied IR-luminous populations: they contain greater proportions of hot dust, with a characteristic dust temperature of 60–100 K (Wu et al. 2012; Bridge et al. 2013; Fan et al. 2016a), significantly hotter than the typical 30–40 K observed in SMGs or DOGs (e.g., Melbourne et al. 2012; Magnelli et al. 2012). They are much brighter and rarer than DOGs (there are about 0.03 deg^{-2} versus 300 deg^{-2}). Although not required, for selection using *WISE* colors, they all satisfy the DOG selection criteria (Dey et al. 2008) but are much hotter; therefore, we have dubbed them as "Hot DOGs" (Wu et al. 2012).

Hot DOGs likely host very powerful AGNs, as indicated by their high dust temperatures and SEDs, and the AGN dominates their luminosities (Eisenhardt et al. 2012; Assef et al. 2015; Tsai et al. 2015; Fan et al. 2016a; Farrah et al. 2017). These AGNs have very high extinction, typically $A_V \sim 20$ and up to $A_V \sim 60$ (Assef et al. 2015), and are close to Compton thick in the X-ray bands (Stern et al. 2014; Piconcelli et al. 2015; Assef et al. 2016; Vito et al. 2018). They are likely experiencing very strong feedback: a significant number of such galaxies present extended Lyα blob structures extended over tens of kiloparsecs (Bridge et al. 2013). A recent high spatial resolution [C II] observation with ALMA of the most luminous Hot DOG W2246-0526 reveals an extended, uniform, highly turbulent interstellar medium, indicative of an isotropically expelling galaxy-scale event (Díaz-Santos et al. 2016).

Their high luminosities, hot dust temperatures, and strong feedback suggest that Hot DOGs may be in transition between the obscured and unobscured phases of luminous quasars, when the surrounding dust and gas are being heated and blown out, just before visible quasars emerge (Wu et al. 2012; Bridge et al. 2013; Assef et al. 2015; Díaz-Santos et al. 2016; Fan et al. 2016b). Given the high luminosities for Hot DOGs, the inferred BH mass must be well above the local BH mass–host galaxy correlation if a typical AGN accretion rate is assumed, or, alternatively, the Eddington ratio must be very high, even above the Eddington limit (Assef et al. 2015; Tsai et al. 2015). Potentially both factors may be present. Therefore, a measurement of their BH masses is a key step to understanding Hot DOGs.

Here we present a pilot survey to measure the BH mass of five Hot DOGs at $z \sim 2$ using the line width of the broad Hα line redshifted into the near-IR. A description of the observations and data reduction is given in Section 2, and in Section 3 we fit the line width of the spectra. The estimated BH masses, luminosities, and Eddington ratios are presented in Section 4. In Section 5, we compare Hot DOGs to other galaxy populations at $z \sim 2$, as well as to quasars at $z \sim 6$. Conclusions are summarized in Section 6. Throughout this paper, we assume a ΛCDM cosmology with $H_0 = 70$ km s^{-1} Mpc^{-1}, $\Omega_m = 0.3$, and $\Omega_{\Lambda} = 0.7$.

2. Observations and Data Reduction

We observed five Hot DOGs with secure redshifts and well-sampled SEDs. All selected targets have redshifts $z \sim 2$, so their Hα line is observable with near-IR spectroscopy. Except for requiring coordinates that made them accessible during the observing runs, no other selection criteria were applied when choosing these targets. Their extinctions have been calculated from a model of their rest-frame UV to mid-IR SEDs that includes a starburst, evolved stars, and reddened AGN components (Assef et al. 2015). The derived extinctions range from $A_V \sim 8$ to 25. Source information is listed in Table 1.

Normally at such high extinction, broad-line regions (BLRs) will be hard to see. But for some Hot DOGs we see hints of BLR emission even in the rest-UV (Wu et al. 2012; Assef et al. 2016). This is possibly because AGNs in these Hot DOGs are so luminous compared to their host galaxies, BLR emission leaks through the torus, or could perhaps be due to reflection of BLR emission by dust. A detailed discussion of this leaking/scattering explanation for Hot DOGs is given in Assef et al. (2016), in which a subsample of Hot DOGs have been found to have excess UV/optical emission (blue-excess Hot DOGs, or

Table 1
Target List

Source	R.A.	Decl.	Instrument	Filter	UT Date	Int. Time (minutes)
W0338+1941	03:38:51.33	+19:41:28.6	Keck/MOSFIRE	K	2014 Nov 4	66
W0904+3947	09:04:39.84	+39:47:15.2	Keck/MOSFIRE	K	2014 Nov 4	42
W1136+4236	11:36:34.29	+42:36:02.9	Keck/MOSFIRE	K, H	2014 May 6	18, 30
W2136−1631	21:36:55.74	−16:31:37.8	Keck/MOSFIRE	H	2015 Jun 8	48
W2216+0723	22:16:19.09	+07:23:53.6	Gemini/FLAMINGOS-2	J, H	2014 Nov 7	60

"BHDs"), which can be best explained as unobscured light leaked from the AGN by reflection off dust.

2.1. Keck/MOSFIRE

We obtained near-IR spectroscopy for four Hot DOGs (WISE J033851.33+194128.6, WISE J090439.84+394715.2, WISE J113634.29+423602.9, and WISE J213655.74−163137.8, hereafter W0338+1941, W0904+3947, W1136+4236, and W2136−1631, respectively) using the Multi-Object Spectrometer For Infrared Exploration (MOSFIRE) instrument (McLean et al. 2010, 2012) at Keck Observatory. K-band spectra for three Hot DOGs and H-band spectra for two Hot DOGs were obtained during three runs in 2014 and 2015 (one target was observed in both bands). The MOSFIRE K-band filter is centered at 2.162 μm with an FWHM of 0.483 μm. The H-band filter is centered at 1.637 μm with an FWHM of 0.341 μm. The data were acquired using masks with a slit width of 0″.7, giving a velocity resolution of $\Delta v \sim 80$ km s^{-1} ($R \sim 3600$). Each individual exposure time was 2−3 minutes. The observation dates and total integration times are listed in Table 1. The seeing during the observations was $\sim$0″.5 for W2136−1631 and 1″−1″.2 for the rest of the targets.

The data were reduced using the MOSFIRE data reduction pipeline, which performs flat-fielding, sky subtraction, and wavelength calibration, and outputs rectified 2D spectra, from which 1D spectra were extracted. Telluric correction and flux calibration were performed using the spectra of A0 standard stars.

2.2. Gemini/FLAMINGOS-2

WISE J221648.05+072353.6 (hereafter W2216+0723) was observed using FLAMINGOS-2 (Eikenberry et al. 2012) at the Gemini-South Observatory on the night of UT 2014 November 7. It was observed simultaneously in the J and H bands using the JH grating with the 2 pixel wide (0″.36) long slit, providing a spectral resolving power of approximately $R \sim 1000$. The target was observed for 1 hr in an ABBA sequence. Additional observations were obtained on the nights of UT 2014 June 2, UT 2014 July 13, and UT 2014 November 6 using the same configuration but under much poorer weather conditions, so we do not consider them any further in this analysis.

The data were reduced using standard IRAF[11] tools with the sky emission lines used for wavelength calibration. The star HIP 106817 was used for telluric and flux calibration using the XTellCorr_General routine of the Spextool package (Vacca et al. 2003).

---

[11] http://iraf.noao.edu

3. Line Width Fitting

We detected broad Hα lines in all five Hot DOGs. We modeled the lines using the IDL routine MPFIT (Markwardt 2009). The aim of the fitting is to measure the line width of the Hα line originating from the BLR that is broadened by virial motion, in order to estimate the BH mass (see Section 4.1). There are two major concerns that can affect the fitting result significantly: one is the blending with emission lines from the narrow-line regions (NLRs), while the other is any contribution from outflows. We discuss them separately next.

3.1. Fitting Spectra with Broad Lines and Narrow Lines

The broad Hα line is blended with narrow Hα and [N II] $\lambda\lambda$6549, 6585 emissions, which need to be removed when their contributions are not negligible. We fit the broad line Hα and narrow lines Hα, [N II] $\lambda\lambda$6549, 6585, [O I] $\lambda\lambda$6300, 6364, and [S II] $\lambda\lambda$6717, 6732 simultaneously. We fix the line ratios for the [N II] $\lambda\lambda$6549, 6585 doublets to be 1:2.96 according to Greene & Ho (2005), in order to decompose the possible blending between the Hα and [N II] doublets at relatively low signal-to-noise ratio (S/N). We fit the rest-frame 6000–7000 Å spectra, including a power-law continuum and Gaussian lines, where all the components are limited to have non-negative fluxes and reported line widths are corrected for instrumental resolution. The modeled spectra are plotted in Figure 1. We iterated the fit once to include just the inner 98.76% of the data sorted in absolute value of the residual (2.5σ Gaussian rejection), and we minimized χ_ν^2 over the 6000–7000 Å range.

In this section, we focus on the question whether the broad-line and/or narrow-line components are necessary to fit the near-IR spectra. We explored three strategies to select the best parameterization to fit the spectra. In strategy 1, we only fit one broad Gaussian (FWHM > 1000 km s^{-1}) for Hα, assuming that the narrow Hα and [N II] are negligible compared to the broad Hα ("1B alone" strategy hereafter).

In strategy 2, we fit a single narrow Gaussian (FWHM <1000 km s^{-1}) in addition to a single broad Gaussian to Hα ("1B+1N" hereafter). We kept all narrow line widths the same and allowed the broad component's center to range within $\pm$1000 km s^{-1} from the narrow Hα redshift (e.g., Bonning et al. 2007; Shen et al. 2011), determined from the peak of the narrow-line model fit.

In strategy 3, we allow two broad Gaussians and one narrow Gaussian to fit Hα ("2B+1N" hereafter), with the reported FWHM of Hα derived by the combination of the two broad Gaussians. The second broad component is assumed to have the same redshift as the narrow lines. Combining multiple Gaussians to obtain the broad FWHM has been used in many other works (e.g., Greene & Ho 2005; Assef et al. 2011; Jun et al. 2017). We present the fitted spectra in Figure 1. The fitting parameters, including FWHM, the errors from MPFIT,
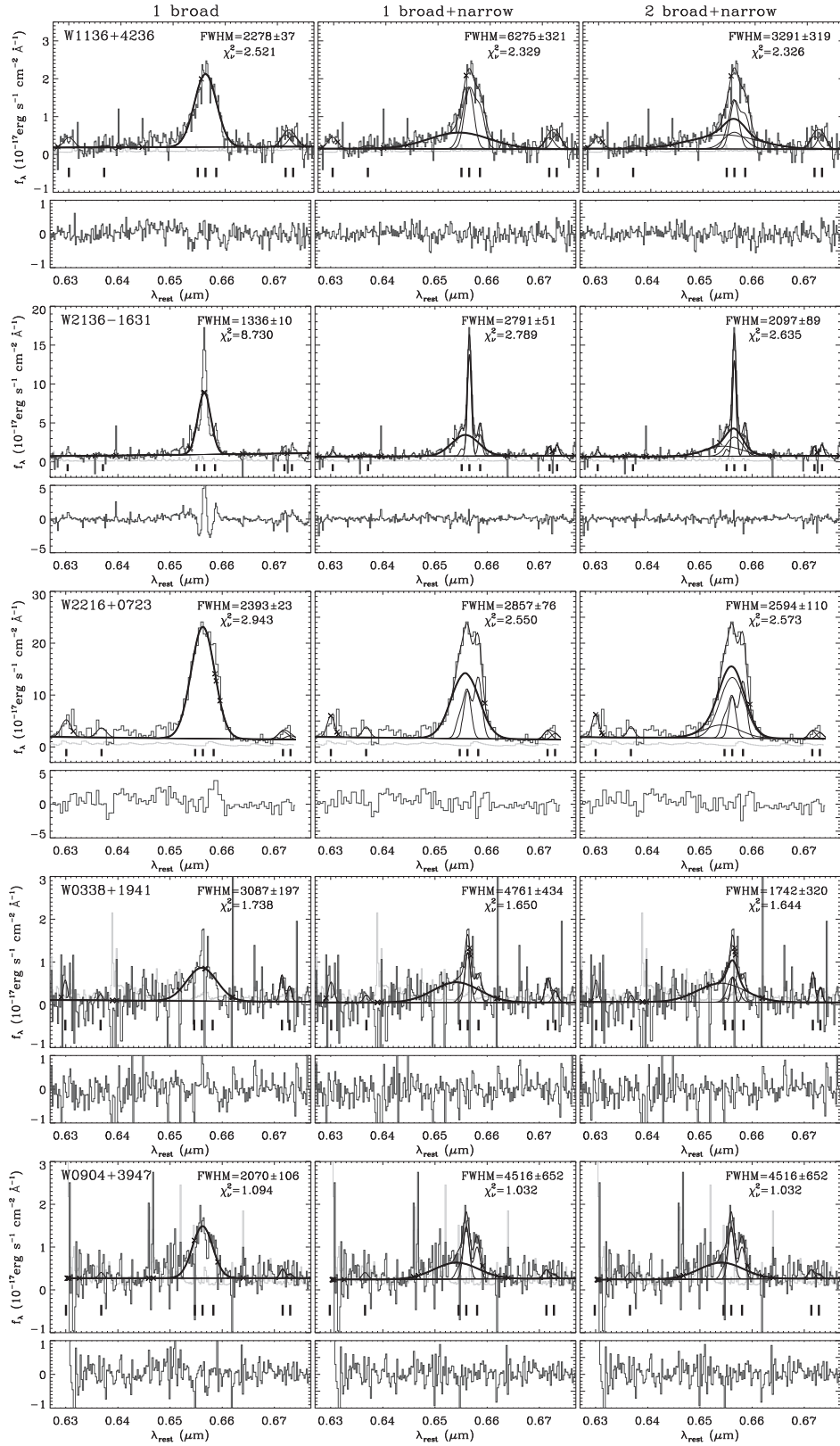
Figure 1. *K*-band spectroscopy for three Hot DOGs and *H*-band spectroscopy for two Hot DOGs with model fits. We binned the spectra to their spectral resolution (∼3 pixels for MOSFIRE, and ∼2 pixels for FLAMINGOS-2) for display purposes. Fitted lines are shown in thick black lines, data are plotted in dark gray, and errors are presented in light gray. The crosses mark rejected pixels. Short vertical lines below the spectra indicate the locations of [O I] $\lambda\lambda6300, 6364$, Hα $\lambda6563$, [N II] $\lambda\lambda6549, 6585$, and [S II] $\lambda\lambda6717, 6732$. The residual spectra are shown in the panels below the spectral panels. The three Hot DOGs with good S/N are shown in the top panels.

Table 2
Fitting Hα with Models

	One Broad			One Broad + One Narrow			Two Broad + One Narrow		
Source	FWHM (km s^{-1})[a]	$\chi^{2}_{\nu'}$ [b]	dof[c]	FWHM (km s^{-1})[a]	$\chi^{2}_{\nu'}$ [b]	dof[c]	FWHM (km s^{-1})[a]	$\chi^{2}_{\nu'}$ [b]	dof[c]
W0338+1941	3087(197)	1.766	271	4761(434)	1.438	268	1742(320)	1.422	266
W0904+3947	2070(106)	1.289	271	4516(652)	1.069	268	4516(652)	1.074	268
W1136+4236	2278(37)	3.442	303	6275(321)	2.618	300	3291(319)	2.509	298
W2136−1631	1336 (10)	24.716	314	2791(51)	3.845	311	2097(89)	3.199	308
W2216+0723	2393(23)	5.529	72	2857(76)	4.067	70	2594(110)	4.178	68

Notes.
[a] Numbers in parentheses are 1σ uncertainties.
[b] $\chi^{2}_{\nu'}$ are calculated within Hα wavelengths (6450–6650 Å); they are different from χ^{2}_{ν} marked in Figure 2, which are calculated over the entire fitting region.
[c] Degrees of freedom in fitting.

$\chi^{2}_{\nu'}$ (χ^{2}_{ν} calculated only covering Hα wavelengths: 6450–6650 Å), and the degrees of freedom (dof) of the best-fit model for each strategy, are listed in Table 2.

To determine which strategy works best, we applied an F-test to each spectrum over rest frame 6450–6650 Å. The results are listed in Table 3. The values in Table 3 show the probability p that the χ^{2}_{ν} of the fit with the larger number of components was consistent with being drawn from the same distribution as the fit with the smaller number of components. Generally, when $p < 0.05$, we can assume that an extra component is necessary in the fitting. Note that when $p = 0$, it means that the number is so small that it is below the numerical precision of the integrator we used.

Based on Tables 2 and 3, the option 1 "1B alone" strategy is ruled out by the F-test analysis, for all five targets, implying that the narrow-line component is not negligible. (A "one narrow line alone" [1N alone] case versus "1B + 1N" is also rejected by the F-test.) Both broad-line and narrow-line components are necessary to represent the spectra.

As seen in Figure 1, W0338+1941 and W0904+3947 have poorer S/Ns than the other three targets. According to the F-test, the 2B+1N model is strongly preferred in two of the three high-S/N targets. Since all Hot DOGs are arguably physically similar, we assumed that a consistent model should apply to all targets. In this paper we use the 2B+1N model to fit all sources. For the one high-S/N Hot DOG (W2216+0723) where the 2B+1N model is not preferred over the 1B+1N model by the F-test, the resulting FWHMs and implied BH masses for the two models are consistent (see Table 2).

We adopt the FWHM and χ^{2}_{ν} from the 2B+1N model in MPFIT as best-fit values for each target, and then we estimate the error of this best-fit FWHM using a Monte Carlo approach similar to that of Assef et al. (2011). For a given spectrum, we first scale the uncertainty of each pixel such that the χ^{2}_{ν} of the best-fit model is equal to 1. We then create 1000 simulated spectra with the same pixel size as the observed spectrum. The value of each pixel in the simulated spectra is randomly drawn from a Gaussian distribution centered at the flux of the best-fit model in that pixel, with a dispersion equal to its scaled uncertainty. We then fit each of the simulated spectra in the same way as described above. The 68.3% confidence interval of the FWHM is obtained from the distribution of the best-fit FWHM to the simulated spectra. Specifically, the range contains 68.3% of the FWHM values below and above the median of the distribution. This uncertainty is listed in Table 4 as the asymmetric 1σ error of the FWHM.

Table 3
F-test Result among Different Spectral Fitting Models

Source	1N vs. 1B+1N	1B vs. 1B+1N	1B+1N vs. 2B+1N
W0338+1941	3.3e−6	2.8e−7	0.24
W0904+3947	3.9e−5	3.7e−9	1.00
W1136+4236	1.8e−9	1.0e−12	8.8e−3
W2136−1631	0	0	1.3e−11
W2216+0723	3.0e−4	9.5e−6	0.62

3.2. Can Outflows Explain the Broad Hα Line?

Massive outflows have been discovered in some high-redshift, dust-obscured quasars, revealed by the high velocity dispersion of forbidden lines (e.g., Liu et al. 2013, 2014; Zakamska et al. 2016), sometimes accompanied by blueshifted wings. These features have been explained as a manifestation of strong AGN feedback (e.g., Spoon & Holt 2009; Mullaney et al. 2013; Zakamska & Greene 2014; Brusa et al. 2015). In this section, we test whether the broad Hα lines detected in these Hot DOGs can be explained by outflow combined with emission from NLRs.

We obtained H-band spectroscopy for W1136+4236 and detected broad [O III] $\lambda\lambda4959, 5007$ lines. We also obtained J-band spectroscopy for W2216+0723, with broad [O II] $\lambda\lambda3726, 3729$ lines detected. The spectra are presented in Figure 2. Both the [O III] and [O II] doublets are thought to be outflow tracers in quasars (e.g., Zakamska & Greene 2014; Perna et al. 2015). We fit Gaussian profiles for the [O III] and [O II] lines. For W1136+4236, two Gaussians with the same FWHM were fit to the [O III] $\lambda\lambda4959, 5007$, with an FWHM of 2310 km s^{-1}. For W2216+0723, we fit a single Gaussian to the [O II] $\lambda\lambda3726, 3729$ doublet, finding an FWHM of 2607 km s^{-1}. Both these forbidden lines are very broad and present blueshifted wing features, implying that there is outflow in both targets.

The broad Hα we observe in these Hot DOGs can be either caused by virial motion in BLRs right around the massive BHs or from more extended NLRs combined with outflows. We performed the following tests to see which scenario is preferred by the data. In test 1, we fit a single Gaussian line profile to both the oxygen and Hα lines, fixing the line width to be the same as [O III] $\lambda\lambda4959, 5007$ in W1136+4236 and the same as [O II] $\lambda\lambda3726, 3729$ in W2216+0723 (Figure 2), assuming that the lines are broadened only by outflows. The resulting χ^{2}_{ν} values are notably worse than the corresponding models in the 1B+1N and/or 2B+1N models shown in Figure 1. In addition,

Table 4
Derived Parameters of Hot DOGs

Source	z[a]	A_V	FWHM (km s^{-1})	L_{5100} (erg s^{-1})	log(BH Mass)[b] (log$M_\odot$)	$L_{\rm bol}$[c] ($L_\odot$)	η[b]
W0338+1941	2.123	15.5	1742^{+1144}_{-518}	3.40×10^{46}	$8.77^{+0.46}_{-0.25}$	2.8×10^{13}	$1.46^{+2.83}_{-0.66}$
W0904+3947	2.097	8.9	4516^{+812}_{-689}	2.10×10^{46}	$9.51^{+0.17}_{-0.16}$	2.7×10^{13}	$0.25^{+0.14}_{-0.08}$
W1136+4236	2.409	7.8	3291^{+1715}_{-1194}	2.85×10^{46}	$9.30^{+0.39}_{-0.29}$	2.7×10^{13}	$0.62^{+0.91}_{-0.31}$
W2136−1631	1.659	24.8	2097^{+162}_{-166}	1.30×10^{46}	$8.72^{+0.11}_{-0.11}$	2.5×10^{13}	$1.47^{+0.55}_{-0.40}$
W2216+0723	1.685	17.1	2594^{+222}_{-497}	2.90×10^{46}	$9.09^{+0.12}_{-0.18}$	3.0×10^{13}	$0.74^{+0.29}_{-0.27}$

Notes.
[a] Redshifts listed are derived from the spectra presented in this work. The uncertainty of the redshifts is $\Delta z \sim 0.002$.
[b] Uncertainties listed here only consider the measurement uncertainties from the FWHM and the continuum luminosity.
[c] The uncertainty of the bolometric luminosities is 20%.

the resulting line profiles of the [O I] and [S II] lines in this model are too wide to fit the data. In test 2, we used the asymmetric line profile of [O II] $\lambda\lambda3726,3729$ to fit Hα in W2216+0723 (a similar fit to the [O III] $\lambda\lambda4959, 5007$ lines in W1136+4236 did not converge). This led to an even worse χ^2_ν.

In the discussion above, we assume that the outflow occurs in the NLRs. This is a plausible scenario to test if outflow from NLRs can cause the observed Hα line. Although we cannot fully exclude the possibility that outflows contribute to the observed broad Hα, our analysis shows that the 1B+1N and 2B+1N models, where the Hα lines are broadened by the virial motion from BLRs, provide a better fit to our data than the two test models, where the Hα profiles are broadened by NLR outflows.

Even if strong NLR outflows dominate the observed FWHM, preventing us from constraining the BH mass and Eddington ratios in some Hot DOGs, this is still consistent with the picture that Hot DOGs mark a transitional stage in AGN evolution. The detection of very broad [O II] and [O III] lines is intriguing, as the intense outflows this suggests also imply high accretion rates (e.g., Zakamska et al. 2016). Both are expected for the "blowout" phase between the obscured and unobscured quasar stages. While we do not consider BLR outflows in this discussion, we note that strong BLR outflows would likely imply that the virialized BLR component is narrower, which would translate into lower BH masses and, hence, higher, true Eddington ratios.

4. Black Hole Masses, Luminosities, and Eddington Ratios

4.1. Black Hole Masses

BH mass can be estimated by assuming virial equilibrium in the BLR: $M_{\rm BH} \propto v^2 R_{\rm BLR}/G$, where $R_{\rm BLR}$ is the radius of the BLR and G is the gravitational constant. The BLR radius can be measured through the reverberation mapping (RM) technique (e.g., Blandford & McKee 1982; Peterson 1993), which estimates the radius of the BLR from the lag between the variability in the AGN continuum and the corresponding variability in the broad permitted lines. This method has been successful in measuring BH masses in the local universe (e.g., Peterson et al. 2004; Vestergaard & Peterson 2006). For higher-redshift galaxies, BH mass measurements rely on an empirical relation found between the BLR size and the AGN luminosity (the R–L relation) discovered and calibrated by RM studies (i.e., $R_{\rm BLR} \propto L_{5100}^{0.5}$, where $L_{5100} = \lambda L_\lambda$ at $\lambda = 5100$ Å; Kaspi et al. 2000; Bentz et al. 2006, 2009, 2013), which are called "single-epoch" BH mass measurements. Thus, by measuring

rest-frame optical broad-line width and adjacent continuum luminosity, one can estimate the single-epoch BH mass.

Typically used broad lines to calculate high-redshift AGN BH mass include Hα, Hβ, Mg II, and C IV, with Hα and Hβ generally regarded as more reliable. The Hβ line has primarily been used to calibrate the R–L relation based on RM measurements, and the Hα emission line widths and luminosities correlate well with those of Hβ over a wide range of total AGN luminosities (e.g., Greene & Ho 2005; Jun et al. 2015), supporting the use of Hα whenever available. Since Hα emission is several times stronger than Hβ (Shen & Liu 2012; Jun et al. 2015) and is less blended with broad Fe II emission than Hβ, it is especially preferred for spectroscopy of fainter AGNs. At $z \gtrsim 1$, Balmer emission is redshifted out of the optical window, so rest-frame UV emission (Mg II, C IV) has been used to measure BH masses. However, concerns about the scatter of the C IV-derived BH masses compared to those derived from Balmer lines (e.g., Assef et al. 2011; Shen & Liu 2012), as well as strong Fe II blending near Mg II, favor using Hα if possible. Moreover, for heavily obscured AGNs like Hot DOGs, UV broad lines are hard to detect. The stronger line and redder wavelength of Hα make it a better choice than other lines to probe BLRs in Hot DOGs.

Following Assef et al. (2011), we calculate the BH mass based on the FWHM of broad-line Hα:

$$M_{\rm BH} = 7.68 \times 10^6 f \left(\frac{{\rm FWHM}_{{\rm H}\alpha}}{10^3 \text{ km s}^{-1}} \right)^{2.06} \times \left(\frac{L_{5100}}{10^{44} \text{ erg s}^{-1}} \right)^{0.52} M_\odot,$$

where f is a scale factor of order unity that depends on the structure, kinematics, and inclination of the BLR (e.g., Collin et al. 2006). Here we adopt the best-fit fixed f factor of 1.17 following the arguments in Assef et al. (2011). Due to the very high UV/optical extinction of Hot DOGs, we cannot use direct measurements of L_{5100}. Instead, we adopt the rest-frame UV to mid-IR SED models for Hot DOGs reported in Assef et al. (2015), which are constrained by WISE and follow-up optical and near-IR photometry, fitting the contributions of a starburst, evolved stars, and reddened AGN components, and derive the obscuration-corrected AGN luminosity. The derived extinctions (A_V) from this model and the resulting BH masses for the five Hot DOGs with broad Hα line measurements are presented in Table 4.

Due to the low S/N for the two Hβ lines detected in W1136+4236 and W2216+0723, we cannot decompose the broad and narrow components for Hβ, complicating the use of the
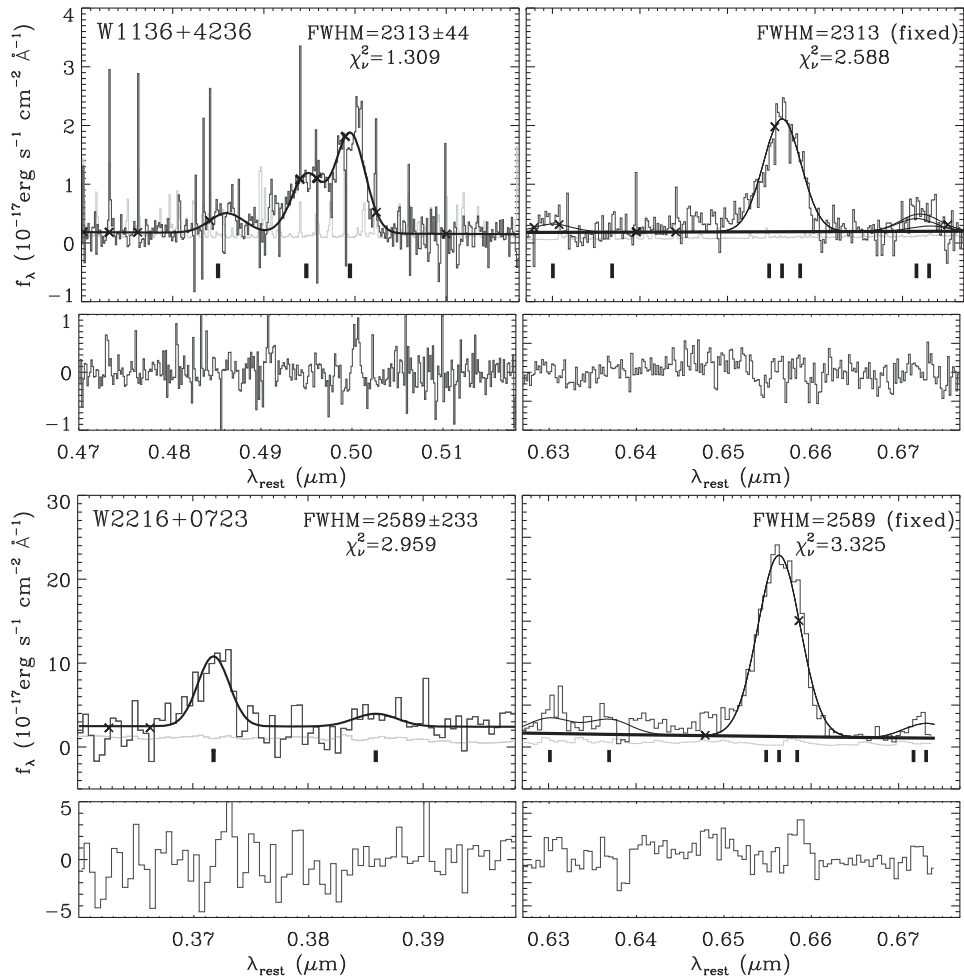
Figure 2. Top panels: H- and K-band spectra for W1136+4236 with model fits. We use Gaussians to fit the Hβ and [O III] $\lambda\lambda$4959, 5007 lines in the H-band spectrum (top left). In the K-band spectrum (top right), we use Gaussians to fit [O I]λ6300, Hα λ6563, and [S II] $\lambda\lambda$6717, 6732, forcing all line widths to the same width as [O III] in the H band. Bottom panels: J- and H-band spectroscopy for W2216+0723 with model fits. We fit one Gaussian for the [O II] $\lambda\lambda$3726, 3729 lines (bottom left) and apply the same line width to fit [O I] and Hα in the H band (bottom right). All fitted lines are shown in thick black lines, data are plotted in dark gray, and errors are presented in light gray. The residual spectra are shown in the panels below the spectral panels. Vertical lines below the spectra show the positions of the Hβ λ4861 and [O III] $\lambda\lambda$4959, 5007 lines in the left panels and the [O I] $\lambda\lambda$6300, 6364, Hα λ6563, [N II] $\lambda\lambda$6549, 6585, and [S II] $\lambda\lambda$6717, 6732 lines in the right panels.

Balmer decrement to estimate extinction. In addition, the possibility that the broad lines are observed owing to scattering (Assef et al. 2016) makes the Balmer decrement method potentially problematic. If we assume the same broad-to-narrow component ratio for Hα and Hβ, the BLR extinction for the two sources predicts a much lower AGN luminosity than what we estimated from the observed SED, implying that the Balmer decrement method is not a reliable way to estimate the extinction for our sample.

4.2. Uncertainties of Black Hole Masses

We estimate the measurement uncertainties in our BH mass calculations by propagating the errors in the FWHM and in the continuum luminosities. The uncertainty in FWHM varies from 8% to 66% owing to differing data quality. We assume a consistent 50% uncertainty in calculating L_{5100} from the SED model (Assef et al. 2015). We assume a 20% uncertainty on the bolometric luminosities (Tsai et al. 2015). The resulting measurement uncertainties are presented in Table 4 and are folded into the error bars in all the figures.

Some authors (e.g., Jun et al. 2015) also consider measurement errors from the f factor (43% following Collin

et al. 2006) and the R–L relation (7%; Bentz et al. 2013). This leads to an additional 0.16 dex uncertainty for BH masses and 0.18 dex uncertainty for Eddington ratios. There are also systematic errors for the constants, which are about 0.3–0.4 dex for the f factor (Kormendy & Ho 2013; McConnell & Ma 2013) and 0.11 dex for the R–L relation (Peterson 2010).

The uncertainties discussed above do not include the uncertainty introduced by the possible contribution of outflows to the FWHM of Hα. As described in Section 3.3, including an outflow component based on the observed [O III] and [O II] lines for W1136+4236 and W2216+0723, respectively, in modeling their broad Hα line profiles leads to a poorer χ_ν^2. To quantitatively estimate the contribution of outflows to FWHM values will require higher-S/N spectra, but it is not expected to significantly affect the results presented here.

4.3. Bolometric Luminosities

Using extensive follow-up photometry (Griffith et al. 2012; Wu et al. 2012; Jones et al. 2014; Assef et al. 2015; Tsai et al. 2015; C. Tsai et al. 2017, in preparation), we constructed complete SEDs for the Hot DOGs and calculated their bolometric luminosities. The method we used is described in

detail in Tsai et al. (2015). In brief, we simply integrated over the detected photometric data points from the optical to far-IR bands, using power-law interpolations between measurements, and extrapolated to 20% beyond the shortest and longest wavelengths. This method is more secure than bolometric luminosities simply scaled up from one or a few wavelength measurements using templates, but it is conservative since it may miss flux between data points and beyond the longest/ shortest wavelength data. If the best-fit SED templates or spline-smoothed SEDs are considered, the luminosities typically increase by 20% (Tsai et al. 2015).

We list the derived bolometric luminosities of the five Hot DOGs in Table 4. The photometry of the Hot DOGs (including the five reported in this paper) observed from *Spitzer* (Griffith et al. 2012), *WISE*, and *Herschel*, as well as more details on the method used to calculate their bolometric luminosities (in which we consider that BH accretion is dominating the luminosity), is reported in C. Tsai et al. (2017, in preparation).

4.4. Eddington Ratios

The Eddington luminosity is defined as

$$L_{\rm Edd} = 3.28 \times 10^4 \left(\frac{M_{\rm BH}}{M_\odot}\right) L_\odot,$$

and the Eddington ratio is $\eta = L_{\rm AGN}/L_{\rm Edd}$. For Hot DOGs, we can attribute most of the bolometric luminosity to the AGN (Eisenhardt et al. 2012; Jones et al. 2014; Díaz-Santos et al. 2016; Farrah et al. 2017; C. Tsai et al. 2017, in preparation). Hence, we calculated Eddington ratios as $L_{\rm bol}/L_{\rm Edd}$ for the five Hot DOGs (see Table 4). We found that η from high-S/N targets are greater than 0.5 and close to unity. Considering that $L_{\rm bol}$ is calculated conservatively, we conclude that the derived Eddington ratios are close to or above the Eddington limit for these Hot DOGs.

5. Discussion

Based on their SEDs and far-IR/mid-IR luminosity ratios, Wu et al. (2012) speculated that Hot DOGs may represent a transitional phase following the SMG and DOG phase and preceding the regular quasar phase. Progression along such a sequence is consistent with galaxy evolution scenarios based on major mergers (e.g., Hopkins et al. 2008) and is likely driven by the growth of the central SMBH.

The primary objective of this study is to measure the BH masses of Hot DOGs and to test whether such an evolutionary sequence is reasonable by comparing their BH masses to those of other populations. The project is also intended to find out whether the high luminosities of Hot DOGs result from hosting BHs with masses well above the local BH–host galaxy relation, and/or whether their SMBHs are accreting at or even above the Eddington limit. To explore these topics, we compare Hot DOGs to other galaxy populations with measurements of BH masses and Eddington ratios. The discussion is organized as follows: We summarize $z \sim 2$ comparison samples and compare them to Hot DOGS in Section 5.1. We discuss possible biases in our results due to our small sample and line-fitting approach in Section 5.2. In Section 5.3, we discuss why Hot DOGs are so luminous among quasars, and in Section 5.4 we describe a possible accretion history of $z \sim 2$ quasars. In

Section 5.5, we compare Hot DOGs to $z \sim 6$ quasars, and we propose that Hot DOGs may exist at other redshifts in Section 5.6.

5.1. Comparison Samples at $z \sim 2$

Comparison populations that may relate to Hot DOGs include normal quasars, SMGs, DOGs, and red quasars. Caution should be used, however, when comparing luminosities of obscured and unobscured populations, since, owing to obscuration, some energy output could be missed by scattering to other directions or be reprocessed to unobserved wavelengths. The extinction correction has to be considered when calculating AGN luminosities used to estimate BH masses and Eddington ratios. For Hot DOGs, we argue that the UV photons have been efficiently converted into mid-IR emission with almost no loss (e.g., Tsai et al. 2015), and we have collected optical to submillimeter SEDs, so that the integrated luminosity should give a good estimate of the bolometric luminosity and can be compared to total luminosities of other populations.

For normal, unobscured quasars, we use the sample of Shen et al. (2011), who collected redshifts and estimated BH masses for more than 100,000 SDSS quasars from the SDSS DR7 spectroscopic quasar catalog (Abazajian et al. 2009; Schneider et al. 2010). Shen et al. (2011) calculated AGN luminosities by scaling up type 1 AGN templates using UV continuum measurements, which is reasonable, as SDSS quasars generally have low extinction. Their sample covers quasars with redshifts $z \sim 0$–5 and includes measured FWHMs of multiple lines (Hα, Hβ, Mg II, and C IV) when they are redshifted into the SDSS spectroscopic range. We are most interested in quasars around $z \sim 2$ that can be directly compared to Hot DOGs in this paper. For SDSS quasars, we prefer to use BH masses derived from Mg II rather than from C IV over this redshift range, since Mg II is the less complicated line to use as a tool for measuring BH masses (e.g., Shen et al. 2008, 2011; Assef et al. 2011; Jun et al. 2015).

The BH mass estimate for SMGs is complicated, partly due to the large uncertainty in determining the AGN luminosity in SMGs. Unlike Hot DOGs, the luminosities of SMGs are generally dominated by starbursts rather than AGNs, though some SMGs are actually 850 μm selected dusty quasars with large extinction. In this paper, we simply adopt average values for general SMGs (whose luminosities are still dominated by starbursts) from Alexander et al. (2008) of $\log (M_{\rm BH}/M_\odot) \sim 8.0$ and $\eta \sim 0.2$.

Melbourne et al. (2011) report the BH masses of four power-law DOGs based on broad Hα measurements. Two of these (DOG 1 and DOG 4) have reliable bolometric (8–1000 μm) luminosities from SED integration including *Herschel* data (Melbourne et al. 2012). Since the AGN contribution is believed to dominate the SED of power-law DOGs, we approximate their AGN luminosities using their bolometric luminosities to calculate Eddington ratios, as we did for Hot DOGs. Melbourne et al. (2011) note that their derived BH masses are lower limits owing to the uncertainty in dust correction. In addition, AGNs in DOGs are less dominant than those in Hot DOGs, and the starburst contribution to the luminosity may not be negligible. Therefore, the derived Eddington ratios for these DOGs are upper limits.
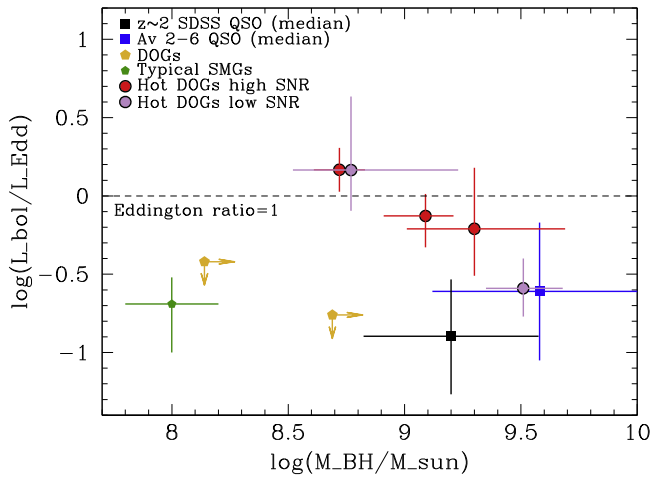
Figure 3. BH masses and Eddington ratios for the five Hot DOGs reported in this paper, compared to typical values for $z \sim 2$ SMGs (Alexander et al. 2008), DOGs (Melbourne et al. 2011), and quasars (Shen et al. 2011; Banerji et al. 2012). Note that the Eddington ratios of Hot DOGs are likely 20% (0.08 dex) higher in general, due to our conservative method in calculating bolometric luminosities. The uncertainties of Hot DOGs shown in the figure only consider the measurement errors from the FWHM and the AGN luminosity. An additional error of 0.16 dex on BH mass and 0.18 dex on Eddington ratio should be added if the systematic errors from the f factor and the R–L relations are considered.

There is growing interest in the study of red quasars, which are thought to be a linking population between obscured and unobscured quasars (e.g., Glikman et al. 2012; Ross et al. 2015). Initially, red quasars were selected using optical/near-IR colors (e.g., Richards et al. 2003) and some cross-matching to radio surveys (e.g., Glikman et al. 2007, 2015). With the large-area, deep mid-IR imaging surveys available from *Spitzer* and *WISE*, additional mid-IR color cuts have been found to be very efficient in selecting red quasars (e.g., Banerji et al. 2013, 2015; Ross et al. 2015; Hamann et al. 2017). These red quasars normally have moderate extinctions ($E(B - V) < 1.5$). We adopt the luminosities and Eddington ratios from the red quasar sample of Banerji et al. (2012, 2015), the largest red quasar sample ($A_V \sim 2 - 6$) at $z \sim 2$ that has BH masses measured using broad Balmer lines. Like Shen et al. (2011), Banerji et al. scaled type 1 AGN templates using UV continuum measurements to derive bolometric luminosity, but they have corrected the $5100\,\text{Å}$ luminosity using the obscuration derived from SED fitting.

In Figure 3, we compare the BH masses and Eddington ratios of Hot DOGs to two DOGs, quasars with moderate obscuration, and type 1 quasars. A median value is given for each category of quasar. We also mark the likely ranges of BH masses and Eddington ratios for general SMGs reported in Alexander et al. (2008). The Hot DOGs and comparison samples in Figure 3 have redshifts $z \sim 2$ and BH mass measurements obtained from broad Balmer lines, except for the type 1 SDSS quasars from Shen et al. (2011). Figure 3 shows that the Hot DOGs reported here have higher BH masses than general SMGs or DOGs, based on the limited information available, and are comparable to quasars. The Hot DOGs show systematically higher Eddington ratios than other populations at $z \sim 2$, with values close to unity. Our pilot project supports the idea that Hot DOGs are a transitional, high-accretion phase between obscured and unobscured quasars.
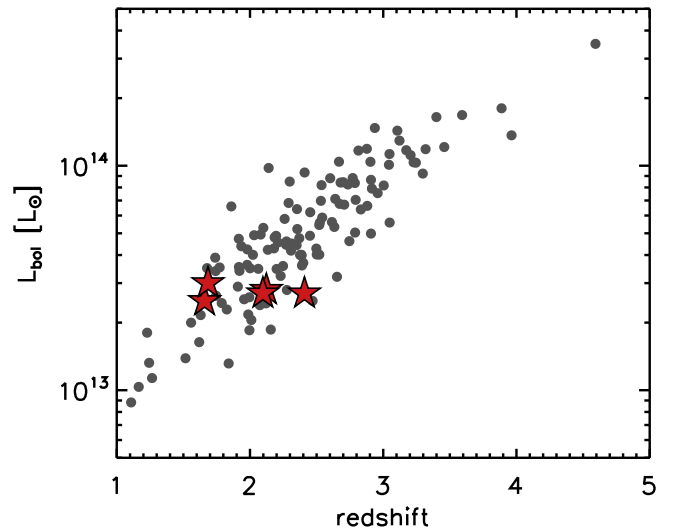
Figure 4. Distribution of redshifts and luminosities of the five Hot DOGs reported in this paper (red stars), compared to the sample of Hot DOGs with *Herschel* measurements (black dots) presented in Figure 1 of Tsai et al. (2015).

5.2. Biases due to Source Selection and Line Fitting

5.2.1. Possible Selection Effects for the Pilot Sample

Our pilot project to calculate BH masses and Eddington ratios is based on five Hot DOGs. We did not impose any selection criteria apart from redshift, but the small sample size raises the question of how well they represent the BH masses and Eddington ratios for the whole Hot DOG population.

In Figure 4 we compare the distribution of redshifts and luminosities of the five Hot DOGs in this paper with all Hot DOGs with redshifts and *Herschel* measurements. Their luminosities are near or somewhat below the median values of Hot DOGs at similar redshifts and are lower than most Hot DOGs. Hence, the Eddington ratios of these five Hot DOGs may be somewhat lower than for typical Hot DOGs with similar BH masses, and it is unlikely that there is a selection bias for a high Eddington ratio subsample because of higher luminosity.

Compared with the obscuration values reported in Assef et al. (2015), two of the five targets are close to the lower limit of extinction values, two are close to the median value, and one is close to the upper limit. Overall, there is no obvious bias in extinction.

Although we did not select targets to have broad UV lines, two (W0904+3947 and W1136+4236) out of the five targets do show broad rest-UV spectra features, which may suggest the direct detection of the BLR in the rest-UV. This 40% ratio is somewhat higher than the 12%–16% fraction of Hot DOGs in general with broad rest-UV lines (Eisenhardt et al., in preparation). The relationship between the detection of BLR in rest-optical and rest-UV bands is not clear, but if we assume a higher chance of detecting broad Hα for sources with broad rest-UV lines, our pilot sample may be biased against Hot DOGs with narrower or less obvious broad UV lines. But for a fixed AGN continuum, this means a bias against smaller FWHMs, lower BH masses, and higher Eddington ratios.

In summary, the possible selection effect of the five Hot DOGs in this paper, including luminosities, obscurations, and existing rest-UV spectra, either has little influence or suggests even higher Eddington ratios for typical Hot DOGs. These
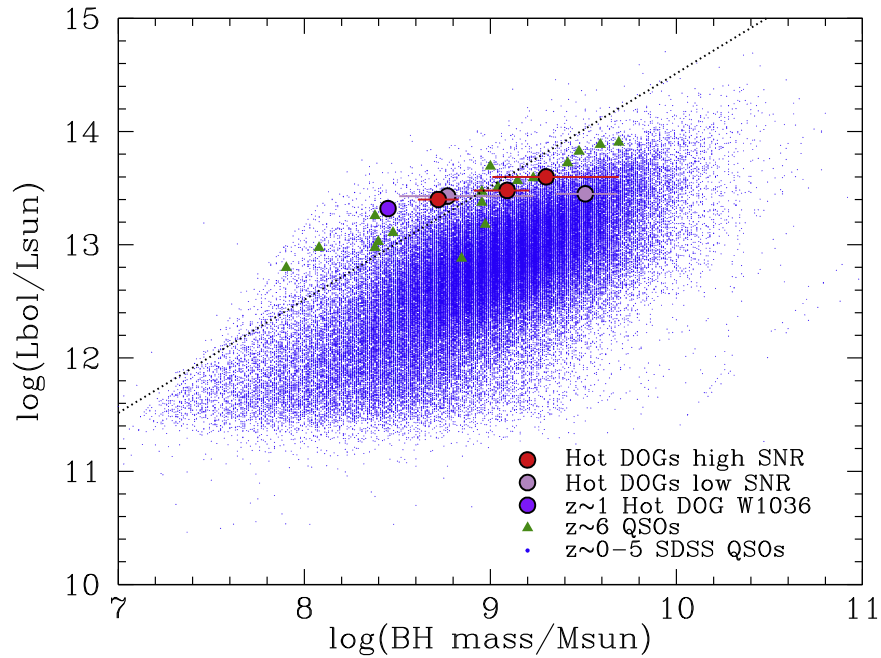
Figure 5. Comparison of BH masses and bolometric luminosities of Hot DOGs and SDSS quasars at $z < 5$ (Shen et al. 2011) and known $z \sim 6$ quasars (Willott et al. 2010; De Rosa et al. 2011). The dotted line traces Eddington ratio $= 1$. Both Hot DOGs and $z \sim 6$ quasars trace the maximum luminosities for quasars at each BH mass. Note that the bolometric luminosities of Hot DOGs in this plot are likely 20% (0.08 dex) higher in general, due to our conservative method in calculating bolometric luminosities. The BH uncertainties of Hot DOGs shown in the figure only consider the measurement errors from the FWHM and the AGN luminosity. An additional error of 0.16 dex should be included If one considers the measurement errors from the f factor and the R–L relations.

considerations are unlikely to change our conclusion that Hot DOGs represent a high Eddington ratio population.

5.2.2. Influence of Different Line-fitting Approaches

The S/Ns of our five spectra vary significantly. Our line-fitting strategy of using a consistent multi-Gaussian fit takes advantage of the high-S/N spectra, and our approach of using spectral information as a prior in Monte Carlo simulation with an F-test investigation gives a robust and sensitive way to deal with the low-S/N spectra and variations between models for some targets. However, some authors prefer to use a simpler approach for lower-S/N spectra, namely, selecting the simplest Gaussian model with a small enough χ^2. How would our results change if we were to take this simpler approach?

From Table 2 and Figure 1, the simplest Gaussian model with a reasonable χ^2 would select the 1B model for all targets except for W2136-1631, for which the 1B+1N model is required. If these models are selected, two targets (W0338 +1941, W2136-1631) have larger BH masses and lower Eddington ratios, and the other three targets have lower BH masses and higher Eddington ratios. The Eddington ratios range from 0.25–1.46 to 0.45–1.31, with the median value changing from 0.74 to 0.88. The overall effect is to move the derived Eddington ratios of Hot DOGs toward unity. Again, this does not change our major conclusion that Hot DOGs are a high Eddington ratio population.

5.3. Why Are Hot DOGs So Luminous: Comparing to SDSS Quasars

In the previous section, we showed that Hot DOGs tend to have higher Eddington ratios than other IR-luminous (active) galaxy populations at $z \sim 2$. Here we argue that an unusually high accretion rate is characteristic of Hot DOGs and is not a

selection effect. In Figure 5, we compare the BH masses and bolometric luminosities for Hot DOGs to SDSS quasars at all redshifts ($z = 0$–5) from Shen et al. (2011), which is the largest and least biased quasar sample with BH masses in the literature. We also include a lower-redshift ($z = 1.009$) Hot DOG (WISE J1036+0449) newly reported in Ricci et al. (2017).

Hot DOGs roughly trace the upper luminosity boundary of the SDSS quasar distribution in Figure 5. In other words, they are near the maximum bolometric luminosities seen in quasars with similar BH masses. Such high luminosities must come from very efficient BH accretion. The corresponding Eddington ratios are close to and may even exceed unity (see Figures 3 and 5). However, the Hot DOGs (especially those with high-S/N spectra) are well away from the high-mass boundary of the SDSS quasar distribution, arguing against the idea that the high Eddington ratios of Hot DOGs are purely a luminosity selection effect.

To highlight this further and reduce possible evolutionary effects, in Figure 6 we zoom in to $z = 1.65$–1.7, where two of the three Hot DOGs with high-S/N spectra fall. The SDSS quasars at these redshifts display a broad distribution of BH masses extending to both sides of the BH masses for the two Hot DOGs, indicating that these Hot DOGs have BH masses typical of normal quasars but luminosities at the top of the range spanned by SDSS quasars. Figures 4 and 5 imply that Hot DOGs have achieved the highest accretion rates that quasars with similar BH masses can reach.

In fact, Hot DOGs appear to compose a significant fraction of the most luminous quasars (Assef et al. 2015) and include the single most luminous galaxy or quasar known (Tsai et al. 2015; Díaz-Santos et al. 2016), suggesting that dust obscuration is an important aspect of maximally accreting SMBHs. However, Hot DOGs are not the only populations to
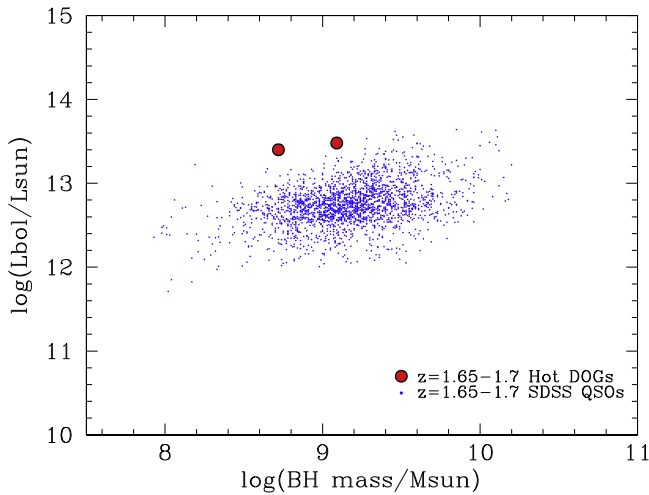
Figure 6. Comparison of BH masses and bolometric luminosities of Hot DOGs and SDSS quasars (Shen et al. 2011) in the redshift range $1.65 < z < 1.70$. The bolometric luminosities of Hot DOGs are likely 20% higher, due to our conservative method in calculating bolometric luminosities.

reach the highest accretion rates for their BH masses. Some optically selected SDSS quasars have comparably high luminosities and Eddington ratios, as do some very high redshift ($z \sim 6$) quasars, as we discuss in Section 5.5.

5.4. A Quasar Accretion History at $z \sim 2$

Hot DOGs likely signify a phase of the highest accretion rate at $z \sim 2$, connecting obscured and unobscured quasars. This scenario is consistent with the expectation of a popular galaxy model in which AGN feedback sweeps out the surrounding material that is also the fuel for BH accretion (e.g., Hopkins et al. 2008; Somerville et al. 2008). We should expect to see less obscured quasars associated with larger SMBHs, as well as with falling accretion rates and fading quasar luminosities. A similar evolutionary connection was also proposed in Assef et al. (2015), based on the luminosity function of Hot DOGs and quasars, that Hot DOGs can be the progenitors of more massive type 1 quasars, in the case in which they are experiencing enhanced BH accretion.

We can test these predictions using our comparison samples. Although we do not know how long each evolutionary stage lasts during this evolution, we can take a snapshot of the $z \sim 2$ universe to statistically explore the BH properties for each comparison population introduced in Section 5.1. We consider the redshift range $1.5 < z < 2.5$, which includes the Hot DOGs in this paper. The peak epoch of quasar density and major merger activities is $z \sim 2$, and observational data at these redshifts are relatively rich. We focus on BH masses derived from Balmer lines if possible, which are observable from ground-based near-IR spectroscopy at these redshifts. For the SDSS quasars that only have optical spectra, we choose BH masses measured from Mg II instead of C IV, as discussed in Section 5.1. This sets an upper limit of $z = 2.25$ for Mg II to be in the SDSS DR7 spectra. Therefore, we have a slightly smaller redshift range of $1.5 < z < 2.25$ for the SDSS quasar sample, which includes 27,761 quasars.

The BH masses and Eddington ratios of Hot DOGs and other comparison samples are plotted in Figure 7. Hot DOGs have among the highest Eddington ratios of all quasars with similar BH masses, much greater than SMGs or DOGs. Red quasars in

Banerji et al. (2012, 2015) have overlapping but generally lower Eddington ratios than Hot DOGs, but higher Eddington ratios than SDSS quasars, given similar BH masses. The overall average Eddington ratio is 0.37 ± 0.44 for these $z \sim 2$ red quasars, less than Hot DOGs that are close to the Eddington limit.

Hot DOGs not only seem to sample the highest accretion phase of this evolution but also are more heavily obscured than other quasars. We compare the Eddington ratios and extinction of Hot DOGs, red quasars, and regular SDSS quasars in Figure 8. Both Eddington ratios and extinctions roughly follow a decreasing trend along the sequence of Hot DOGs, red quasars, and SDSS quasars, suggesting a quasar evolution sequence consistent with the Hopkins et al. (2008) model.

5.5. Comparison to $z \sim 6$ Quasars

The consistently high Eddington ratios of $z \sim 6$ quasars (e.g., Jiang et al. 2007; Willott et al. 2010; De Rosa et al. 2011) distinguish them from other known SMBH systems, except for the Hot DOG population, as well as a small fraction of high Eddington ratio SDSS quasars at lower redshifts. As shown in Figures 5 and 7, both Hot DOGs and $z \sim 6$ quasars have Eddington ratios close to unity, well above most SDSS quasars of similar BH mass. Hot DOGs have a similar luminosity range (10^{13}–$10^{14} L_\odot$) and comparable BH masses to $z \sim 6$ quasars. They are both experiencing high-accretion events, in the process of rapidly building up their BHs.

Assef et al. (2015) explore the BH mass versus host stellar mass ($M_{\rm Sph}$) relation in Figure 7 of their paper, assuming a fixed Eddington ratio of 0.3, which is typical for SDSS quasars. They estimated the stellar masses of Hot DOGs by multiplying the rest-frame luminosity of the host component in the K band by the mass-to-light ratio (M/L) in that band, which depends on many parameters, including star formation history, metallicity, stellar initial mass function, and the contribution of thermally pulsating AGB stars. They used maximum M/Ls for these parameters to estimate the upper limits of the stellar masses. Their results suggested that Hot DOGs may lie well above the local $M_{\rm BH}$–$M_{\rm Sph}$ relation. Based on the present work, we can reasonably change the fixed Eddington ratio to unity and update the $M_{\rm BH}$–$M_{\rm Sph}$ relation for Hot DOGs, as presented in Figure 9. The Hot DOG stellar masses shown in the plot are again upper limits.[12] We mark the three Hot DOGs with high-S/N Hα spectra as red stars in Figure 9, using the BH masses from this work. After these updates, Hot DOGs are closer to the local $M_{\rm BH} - M_{\rm Sph}$ relation, though these stellar-mass estimates are upper limits and their points may move to the left in Figure 9.

Wang et al. (2010) have estimated the BH–host mass relation for $z \sim 6$ quasars, as shown in Figure 9 by green squares. Intriguingly, the region of $z \sim 6$ quasars overlaps with Hot DOGs in the $M_{\rm BH}$–$M_{\rm Sph}$ plot, suggesting that they may be hosted by similar kinds of galaxies. The key elements for AGN systems are their BH masses, host galaxies, and accretion rates. It seems that Hot DOGs and $z \sim 6$ quasars have similarities in all these elements.

---

[12] We also note here that Figure 9 corrects an error in Assef et al. (2015). Assef et al. (2015) stated that they used an initial mass function (IMF) from Conroy et al. (2013), with a higher M/L in the K band than the M/L for a Chabrier (2003) IMF, but mistakenly used the Chabrier (2013) IMF in their Figure 7. Hence, the stellar masses of Hot DOGs shown in Figure 9 in this paper are about a factor of 2 higher than those shown in Figure 7 of Assef et al. (2015).
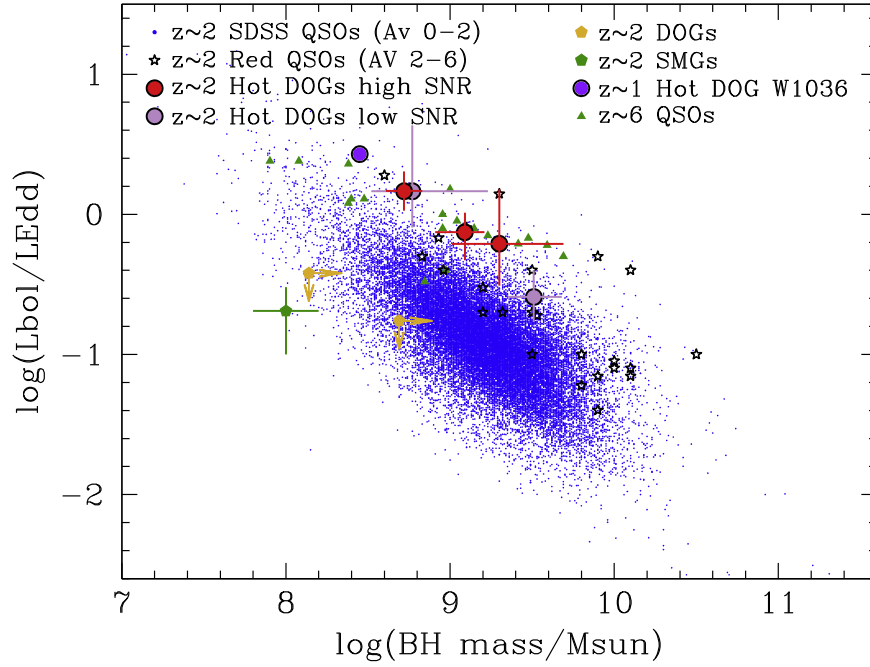
Figure 7. Hot DOGs may trace the highest Eddington ratio stage before the red quasar (Banerji et al. 2012) and SDSS quasar phases (Shen et al. 2011) at redshift $z \sim 2$. The likely range of BH mass and Eddington ratios for general SMGs (Alexander et al. 2008) and the limits for two DOGs (Melbourne et al. 2011, 2012; Shen et al. 2011) are also marked. A $z \sim 1$ Hot DOG (Ricci et al. 2017) and $z \sim 6$ quasars (Willott et al. 2010; De Rosa et al. 2011) are included for comparison. Note that the Eddington ratios of Hot DOGs are likely 20% (0.08 dex) higher, due to our conservative method in calculating bolometric luminosities. The uncertainties of Hot DOGs shown in the figure only consider the measurement errors from the FWHM and the AGN luminosity. An additional error of 0.16 dex on BH mass and 0.18 dex on Eddington ratio should be added if the systematic errors from the f factor and the R–L relations are considered.
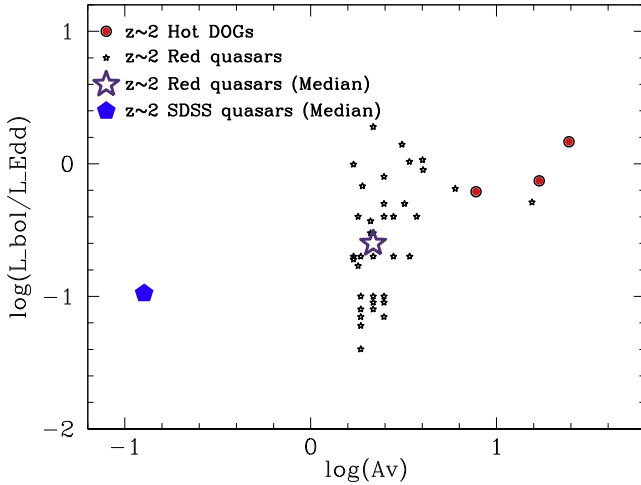
Figure 8. Eddington ratio and extinction for $z \sim 2$ Hot DOGs, SDSS quasars (Shen et al. 2011), and red quasars (Banerji et al. 2012). We only include the three Hot DOGs with good S/N spectra. The median values of SDSS quasars and red quasars are marked with blue and purple symbols, respectively.

The key features of Hot DOGs include high luminosity, high obscuration, hot dust, and high Eddington ratios. Some of these features apply to $z \sim 6$ quasars, too. Significant amounts of hot dust have been revealed in $z \sim 6$ quasars (e.g., Wang et al. 2008; Jiang et al. 2010; Leipski et al. 2014). Hot DOGs at $z = 2$–3 and quasars at $z \sim 6$ may have ultimately been selected for similar reasons: both are experiencing the highest level accretion allowable for their BH masses, leading to hot dust emission and making both the most luminous objects in their own cosmic epochs.

Quasars at $z \sim 6$ are thought to be quite different from lower-redshift quasars (e.g., Willott et al. 2010), not only
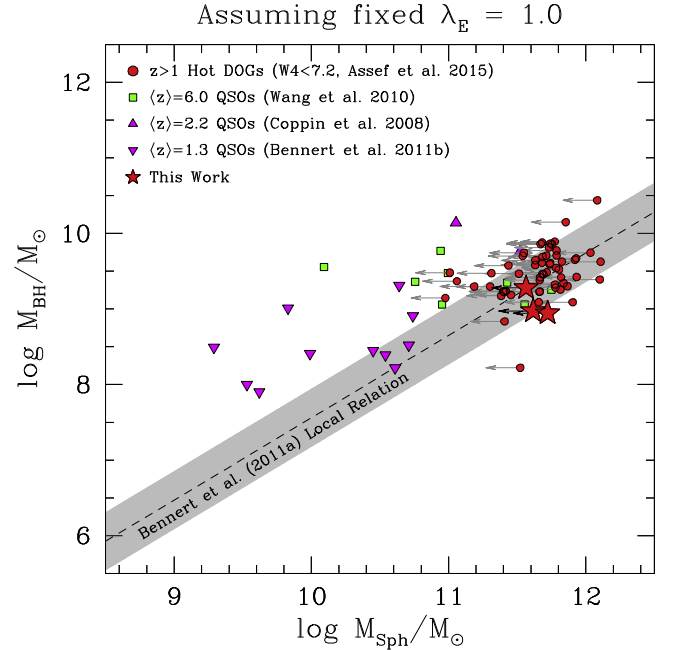
Figure 9. $M_{\rm BH}$ and $M_{\rm Sph}$ values, with Hot DOG data taken from Assef et al. (2015), but assuming a fixed Eddington ratio of 1.0 based on the present work. The high-S/N Hot DOG detections from this work are marked with red stars. The bulge masses of host galaxies are constrained by using the best-fit SED template model of Assef et al. (2011, 2015), which are upper limits. A local relation of active galaxies determined by Bennert et al. (2011), as well as the values for quasars at $z \sim 6$ (Wang et al. 2010), $z \sim 2$ (Coppin et al. 2008), and $z \sim 1.3$ (Bennert et al. 2011), is shown for comparison.

because of their unusually high accretion rates but also because their surrounding environment could be very different. Quasars at $z \sim 6$ represent the earliest generation of SMBHs, when the

gas supply was plentiful. Some have argued that the merger rates were high in the early universe, possibly amenable to spherical accretion (Bondi & Hoyle 1944), and the duty cycle of these SMBHs might have been close to unity (e.g., Willott et al. 2010; Johnson et al. 2012). This is thought to be fundamentally different from lower-redshift SDSS quasars, whose SMBHs have passed their peak accretion, and whose host galaxy gas either will not cool or has been cleared out by AGN feedback (e.g., Di Matteo et al. 2008). Thus, the duty cycle of lower-redshift quasars is much lower. However, we know little about the immediate surrounding environment of SMBHs at $z \sim 6$, except that the host galaxies are dusty. It is possible that SMBHs in Hot DOGs accrete in a similar way to $z \sim 6$ quasars, at least for a short time, resulting in similar accretion efficiencies for systems with comparable BH and host masses. Whether and how BHs in $z \sim 6$ quasars can sustain long-lived Eddington-limited accretion also remains poorly understood. Instead, BHs with multi-episodic, shorter-lived high accretion rate events are both allowed in simulations reproducing the quasar luminosity function (e.g., Hopkins & Hernquist 2010) and suggested in some observations (e.g., Jakobsen et al. 2003; Worseck et al. 2007). Models based on disk accretion for $z \sim 6$ quasars have also been proposed (e.g., Volonteri et al. 2015), predicting short-duty-cycle, highly accreting episodes with very high obscuration.

Compared to $z \sim 6$ quasars, Hot DOGs may represent a later generation (or the peak generation of SMBHs) undergoing their maximum accreting episodes. Spectroscopic studies have revealed that emission-line properties and metallicity do not evolve much from $z \sim 6$ to low-redshift quasars (e.g., Dietrich et al. 2003; Fan et al. 2004; De Rosa et al. 2011). Considering their similarities in BH and host properties, it is possible that the study of Hot DOGs can provide useful constraints and potential insight into understanding the BH accretion and BH–host interaction in $z \sim 6$ quasars.

5.6. A Hot DOG Stage at Different Cosmic Epochs?

We believe that Hot DOGs are heavily obscured AGNs at a special evolutionary stage, characterized by high luminosity owing to high BH accretion rates, and likely with strong AGN feedback. Current work focuses on the studies of $z \sim 2$–3 Hot DOGs. If Hot DOGs trace the transitional, peak accreting phase between obscured and unobscured quasars, should they also exist at other redshift ranges?

Like $z \sim 6$ quasars, Hot DOGs are accreting at the maximum level for their BH masses. However, Hot DOGs are heavily dust obscured, while known $z \sim 6$ quasars are mostly selected from their strong rest-frame UV emission (observed at near-IR wavelengths for the most distant systems) and so are more obviously like highly accreting, optically bright $z \sim 2$–3 SDSS quasars that may have just passed the accretion peak. Hot DOGs may instead be approaching or at the accretion peak. If there are Hot DOGs at higher redshifts, they would be an obscured version of current known $z \sim 6$ quasars. Additional searches using IR photometry available from WISE, Spitzer, and Herschel may help reveal more dusty, higher obscured $z \sim 6$ quasars (Blain et al. 2013), with some promising progress made already (e.g., Wu et al. 2015; Carnall et al. 2015; Wang et al. 2015).

There are more obscured AGNs than unobscured ones in the universe at the same bolometric luminosities (e.g., Stern et al. 2012; Assef et al. 2013). Hot DOGs may signify a key phase linking the well-known unobscured quasar populations to the lesser known world of obscured quasars. The Hot DOG phase may be followed by a high-luminosity, high Eddington ratio red/optical quasar stage, present at all redshifts.

At lower redshifts, Hot DOGs should be rarer owing to the decreasing level of quasar activity. Assef et al. (in preparation) have used a revised WISE color criterion to correct the bias of the Hot DOG selection function against $z < 2$ objects. One successful example is WISE J1036+0449 at $z = 1.009$ (Ricci et al. 2017), whose SED matches well with Hot DOGs, and whose BH mass and Eddington ratio agree with the trends we find in $z \sim 2$ Hot DOGs (Figures 5 and 7). For very low redshift quasars, finding a Hot DOG phase object would be even more interesting, since it would provide a rare opportunity to study those maximally accreting stage SMBHs in more detail. For example, the luminous local quasar PDS 456 at $z = 0.184$ (e.g., Reeves et al. 2000, 2003; Nardini et al. 2015), with a comparable BH mass and luminosity to the $z \sim 2$ Hot DOGs in this paper, also accretes at the Eddington limit. This may be a good example of a post–Hot DOG stage quasar in the local universe. More efforts are needed to search for lower-redshift Hot DOGs, and here WISE data should prove particularly useful.
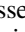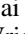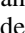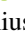
6. Summary

A population of hyperluminous, dusty galaxies has been discovered by WISE, which we call "hot, dust-obscured galaxies" or "Hot DOGs." Their extreme luminosities and hot dust temperatures suggest that they either host very massive BHs well above the local BH mass–stellar mass relation or are accreting at very high rates. We have conducted a pilot survey to measure the BH masses of five Hot DOGs at $z \sim 2$, using MOSFIRE at Keck and FLAMINGOS-2 at Gemini. The primary results from this study are summarized below:

1. Broad Hα lines were detected in all five targets. Spectral fits imply that they are broadened by BLRs around SMBHs. We estimate their BH masses to be $\sim 10^9\,M_\odot$, and their Eddington ratios are close to unity.

2. The BH masses are greater than those of typical SMGs and DOGs and comparable to those of unobscured quasars. This is consistent with the model where Hot DOGs represent a transitional stage between obscured and unobscured quasars. Although not preferred by our spectral fitting, even if strong outflows contribute to the broad line width of Hα, the implied strong feedback still supports Hot DOGs' role in the overall evolutionary picture.

3. Hot DOGs have high luminosities compared to quasars with similar BH masses, which implies that they are accreting at the highest possible rates for their SMBH masses, i.e., they have the highest Eddington ratios observed for quasars and SMBHs.

4. Our results are consistent with a "Hot DOG–red quasar– optical quasar" evolutionary sequence.

5. Hot DOGs and $z \sim 6$ quasars have comparable BH masses and luminosities and possibly M_{BH}–M_{Sph} relations. Their SMBHs both accrete at the maximum observed rates, close to the Eddington limit, making them the most luminous persistent objects in their own cosmic epochs.

ORCID iDs

Jingwen Wu ⦿ https://orcid.org/0000-0001-7808-3756
Hyunsung D. Jun ⦿ https://orcid.org/0000-0003-1470-5901
Roberto J. Assef ⦿ https://orcid.org/0000-0002-9508-3667
Chao-Wei Tsai ⦿ https://orcid.org/0000-0002-9390-9672
Edward L. Wright ⦿ https://orcid.org/0000-0001-5058-1593
Andrew Blain ⦿ https://orcid.org/0000-0001-7489-5167
Daniel Stern ⦿ https://orcid.org/0000-0003-2686-9241
Tanio Díaz-Santos ⦿ https://orcid.org/0000-0003-0699-6083
Brian T. Hayden ⦿ https://orcid.org/0000-0001-9200-8699
Kyle Boone ⦿ https://orcid.org/0000-0002-5828-6211
Parker Fagrelius ⦿ https://orcid.org/0000-0001-6974-5826

References

Abazajian, K. N., Adelman-McCarthy, J. K., Agüeros, M. A., et al. 2009, ApJS, 182, 543
Alexander, D. M., Brandt, W. N., Smail, I., et al. 2008, AJ, 135, 1968
Assef, R. J., Eisenhardt, P. R. M., Stern, D., et al. 2015, ApJ, 804, 27
Assef, R. J., Kochanek, C. S., Ashby, M. L. N., et al. 2011, ApJ, 728, 56
Assef, R. J., Stern, D., Kochanek, C. S., et al. 2013, ApJ, 772, 26
Assef, R. J., Walton, D. J., Brightman, M., et al. 2016, ApJ, 819, 111
Bachetti, M., Harrison, F. A., Walton, D. J., et al. 2014, Natur, 514, 202
Banerji, M., Alaghband-Zadeh, S., Hewett, P. C., & McMahon, R. G. 2015, MNRAS, 447, 3368
Banerji, M., McMahon, R. G., Hewett, P. C., et al. 2012, MNRAS, 427, 2275
Banerji, M., McMahon, R. G., Hewett, P. C., et al. 2013, MNRAS, 429, 55
Bennert, V. N., Auger, M. W., Treu, T., Woo, J.-H., & Malkan, M. A. 2011, ApJ, 726, 59
Bentz, M. C., Denney, K. D., Grier, C. J., et al. 2013, ApJ, 767, 149
Bentz, M. C., Peterson, B. M., Netzer, H., Pogge, R. W., & Vestergaard, M. 2009, ApJ, 697, 160
Bentz, M. C., Peterson, B. M., Pogge, R. W., Vestergaard, M., & Onken, C. A. 2006, ApJ, 644, 133
Blain, A. W., Assef, R., Stern, D., et al. 2013, ApJ, 778, 113
Blain, A. W., Smail, I., Ivison, R. J., Kneib, J. P., & Frayer, D. T. 2002, PhR, 369, 111
Blandford, R. D., & McKee, C. F. 1982, ApJ, 255, 419
Bondi, H., & Hoyle, F. 1944, MNRAS, 104, 273
Bonning, E. W., Shields, G. A., & Salviander, S. 2007, ApJ, 666, 13
Bridge, C., Blain, A., Borys, C., et al. 2013, ApJ, 768, 91
Brusa, M., Feruglio, C., Cresci, G., et al. 2015, A&A, 578, 11
Bussmann, R. S., Dey, A., Borys, C., et al. 2009, ApJ, 705, 184
Bussmann, R. S., Riechers, D., Fialkov, A., et al. 2015, ApJ, 812, 43
Carlstrom, J. E., Ade, P. A. R., Aird, K. A., et al. 2011, PASP, 123, 568
Carnall, A. C., Shanks, T., Chehade, B., et al. 2015, MNRAS, 451, 16
Casey, C. M., Narayanan, D., & Cooray, A. 2014, PhR, 541, 45
Chabrier, G. 2003, PASP, 115, 763
Chapman, S. C., Blain, A., Smail, Ian, & Ivison, R. J. 2005, ApJ, 622, 772
Collin, S., Kawaguchi, T., Peterson, B. M., & Vestergaard, M. 2006, A&A, 456, 75
Conroy, C., Dutton, A. A., Graves, G. J., Mendel, J. T., & van Dokkum, P. G. 2013, ApJL, 776, 26
Coppin, K. E. K., Swinbank, A. M., Neri, R., et al. 2008, MNRAS, 389, 45
De Rosa, G., Decarli, R., & Walter, F. 2011, ApJ, 739, 56
Dey, A., Soifer, B. T., Desai, V., et al. 2008, ApJ, 677, 943
Di Matteo, T., Colberg, J., Springel, V., Hernquist, L., & Sijacki, D. 2008, ApJ, 676, 33
Díaz-Santos, T., Assef, R. J., Blain, A. W., et al. 2016, ApJL, 816, 6
Dietrich, M., Hamann, F., Appenzeller, I., & Vestergaard, M. 2003, ApJ, 596, 817
Donley, J. L., Rieke, G. H., Pérez-González, P. G., Rigby, J. R., & Alonso-Herrero, A. 2007, ApJ, 660, 167
Dowell, C. D., Conley, A., Glenn, J., et al. 2014, ApJ, 780, 75
Eikenberry, S., Bandyopadhyay, R., Bennett, J. G., et al. 2012, Proc. SPIE, 8446, 0I
Eisenhardt, P. R. M., Wu, J., Tsai, C., et al. 2012, ApJ, 755, 173
Fan, L., Han, Y., Fang, G., et al. 2016a, ApJ, 822, 32
Fan, L., Han, Y., Nikutta, R., et al. 2016b, ApJ, 823, 107
Fan, X., Carilli, C. L., & Keating, B. 2006, ARA&A, 44, 415
Fan, X., Hennawi, J. F., Richards, G. T., et al. 2004, AJ, 128, 515
Farrah, D., Lonsdale, C. J., Weedman, D. W., et al. 2008, ApJ, 677, 957
Farrah, D., Petty, S., Connolly, B., et al. 2017, ApJ, 844, 106
Fürst, F., Walton, D. J., Harrison, F. A., et al. 2016, ApJ, 831, 14
Glikman, E., Helfand, D. J., White, R. L., et al. 2007, ApJ, 667, 673
Glikman, E., Simmons, B., Mailly, M., et al. 2015, ApJ, 806, 218
Glikman, E., Urrutia, T., Lacy, M., et al. 2012, ApJ, 757, 51
Greene, J. E., Alexandroff, R., Strauss, M. A., et al. 2014, ApJ, 788, 91
Greene, J. E., & Ho, L. C. 2005, ApJ, 630, 122
Griffith, R. L., Kirkpatrick, J. D., Eisenhardt, P. R. M., et al. 2012, AJ, 144, 148
Hainline, K. N., Hickox, R. C., Carroll, C. M., et al. 2014, ApJ, 795, 124
Hamann, F., Zakamska, N. L., Ross, N., et al. 2017, MNRAS, 464, 3431
Hopkins, P. F., & Hernquist, L. 2010, MNRAS, 402, 985
Hopkins, P. F., Hernquist, L., Cox, T. J., et al. 2006, ApJS, 163, 1
Hopkins, P. F., Hernquist, L., Cox, T. J., & Keres, D. 2008, ApJS, 175, 356
Israel, G. L., Belfiore, A., Stella, L., et al. 2017a, Sci, 355, 817
Israel, G. L., Papitto, A., Esposito, P., et al. 2017b, MNRAS, 466, 48
Jakobsen, P., Jansen, R. A., Wagner, S., & Reimers, D. 2003, A&A, 397, 891
Jiang, L., Fan, X., Brandt, W. N., et al. 2010, Natur, 464, 380
Jiang, L., Fan, X., Vestergaard, M., et al. 2007, AJ, 134, 1150
Johnson, J. L., Whalen, D. J., Fryer, C. L., & Li, H. 2012, ApJ, 750, 66
Jones, S. F., Blain, A. W., Stern, D., et al. 2014, MNRAS, 443, 146
Jun, H. D., & Im, M. 2013, ApJ, 779, 104
Jun, H. D., Im, M., Kim, D., & Stern, D. 2017, ApJ, 838, 41
Jun, H. D., Im, M., Lee, H. M., et al. 2015, ApJ, 806, 109
Kaspi, S., Smith, P. S., Netzer, H., et al. 2000, ApJ, 533, 631
Kleinmann, D. E., & Low, F. J. 1970, ApJ, 159, 165
Kormendy, J., & Ho, L. C. 2013, ARA&A, 51, 511
Leipski, C., Meisenheimer, K., Walter, F., et al. 2014, ApJ, 785, 154

Liu, G., Zakamska, N. L., & Greene, J. E. 2014, MNRAS, 442, 1303
Liu, G., Zakamska, N. L., Greene, J. E., Nesvadba, N. P. H., & Liu, X. 2013, MNRAS, 436, 2576
Lonsdale, C. J., Polletta, M. C., Omont, A., et al. 2009, ApJ, 692, 442
Magnelli, B., Lutz, D., Santini, P., et al. 2012, A&A, 539, 155
Markwardt, C. B. 2009, in ASP Conf. Ser. 411, Astronomical Data Analysis Software and Systems XVIII, ed. D. A. Bohlender, D. Durand, & P. Dowler (San Francisco, CA: ASP), 251
McConnell, N. J., & Ma, C.-P. 2013, ApJ, 764, 184
McLean, Ian S., Steidel, Charles C., Epps, H. W., et al. 2010, Proc. SPIE, 7735, 77351E
McLean, Ian S., Steidel, Charles C., Epps, H. W., et al. 2012, Proc. SPIE, 8446, 84460J
Melbourne, J., Peng, C. Y., Soifer, B. T., et al. 2011, AJ, 141, 141
Melbourne, J., Soifer, B., Desai, V., et al. 2012, AJ, 143, 125
Mullaney, J. R., Alexander, D. M., Fine, S., et al. 2013, MNRAS, 433, 622
Narayanan, D., Dey, A., Hayward, C. C., et al. 2010, MNRAS, 407, 1701
Nardini, E., Reeves, J. N., Gofford, J., et al. 2015, Sci, 347, 860
Negrello, M., Hopwood, R., De Zotti, G., et al. 2010, Sci, 330, 800
Neugebauer, G., Habing, H. J., van Duinen, R., et al. 1984, ApJL, 278, 1
Perna, M., Brusa, M., Cresci, G., et al. 2015, A&A, 574, 82
Peterson, B. M. 1993, PASP, 105, 24
Peterson, B. M. 2010, in IAU Symp. 267, Co-evolution of Central Black Holes and Galaxies, ed. B. Peterson, R. Somerville, & T. Storchi-Bergmann (Cambridge: Cambridge Univ. Press), 151
Peterson, B. M., Ferrarese, L., Gilbert, K. M., et al. 2004, ApJ, 613, 682
Piconcelli, E., Vignali, C., Bianchi, S., et al. 2015, A&A, 574, 9
Pilbratt, G. L., Riedinger, J. R., Passvogel, T., et al. 2010, A&A, 518, 1
Reeves, J. N., O'Brien, P. T., Vaughan, S., et al. 2000, MNRAS, 312, 17
Reeves, J. N., O'Brien, P. T., & Ward, M. J. 2003, ApJ, 593, 65
Ricci, C., Assef, R. J., Stern, D., et al. 2017, ApJ, 835, 105
Richards, G. T., Hall, P. B., Vanden Berk, D. E., et al. 2003, AJ, 126, 1131
Riechers, Dominik A., Bradford, C. M., Clements, D. L., et al. 2013, Natur, 496, 329
Rieke, G. H., & Low, F. J. 1972, ApJL, 176, 95

Rigby, J. R., Rieke, G. H., Maiolino, R., et al. 2004, ApJS, 154, 160
Ross, N. P., Hamann, F., Zakamska, N. L., et al. 2015, MNRAS, 453, 3932
Schneider, D. P., Richards, G. T., Hall, P. B., et al. 2010, AJ, 139, 2360
Shen, Y., Greene, J. E., Strauss, M. A., Richards, G. T., & Schneider, D. P. 2008, ApJ, 680, 169
Shen, Y., & Ho, L. C. 2014, Natur, 513, 210
Shen, Y., & Liu, X. 2012, ApJ, 753, 125
Shen, Y., Richards, G. T., Strauss, M. A., et al. 2011, ApJ, 194, 45
Somerville, R. S., Hopkins, P. F., Cox, T. J., Robertson, B. E., & Hernquist, L. 2008, MNRAS, 391, 481
Spoon, H. W. W., & Holt, J. 2009, ApJL, 702, 42
Stern, D., Assef, R. J., Benford, D. J., et al. 2012, ApJ, 753, 30
Stern, D., Lansbury, G. B., Assef, R. J., et al. 2014, ApJ, 794, 102
Swetz, D. S., Ade, P. A. R., Amiri, M., et al. 2011, ApJS, 194, 41
Trump, J. R., Impey, C. D., & Kelly, B. C. 2011, ApJ, 733, 60
Tsai, C., Eisenhardt, P. R. M., Wu, J., et al. 2015, ApJ, 805, 90
Vacca, W. D., Cushing, M. C., & Rayner, J. T. 2003, PASP, 115, 389
Vestergaard, M., & Peterson, B. M. 2006, ApJ, 641, 689
Vieira, J. D., Marrone, D. P, Chapman, S. C., et al. 2013, Natur, 495, 344
Vito, F., Brandt, W. N., Stern, D., et al. 2018, MNRAS, 474, 4528
Volonteri, M., Capelo, P. R., Netzer, H., et al. 2015, MNRAS, 452, 6
Wang, F., Wu, X., Fan, X., et al. 2015, ApJL, 807, 9
Wang, R., Carilli, C. L., Neri, R., et al. 2010, ApJ, 714, 699
Wang, R., Carilli, C. L., Wagg, J., et al. 2008, ApJ, 687, 848
Willott, C. J., Albert, L., Arzoumanian, D., et al. 2010, AJ, 140, 546
Worseck, G., Fechner, C., Wisotzki, L., & Dall'Aglio, A. 2007, A&A, 473, 805
Wright, E. L., Eisenhardt, P. R. M., Mainzer, A. K., et al. 2010, AJ, 140, 1868
Wu, J., Bussmann, R. S., Tsai, C., et al. 2014, ApJ, 793, 8
Wu, J., Tsai, C., Sayers, J., et al. 2012, ApJ, 756, 96
Wu, X., Wang, F., Fan, X., et al. 2015, Natur, 518, 512
Yan, L., Sajina, A., Fadda, D., et al. 2007, ApJ, 658, 778
Zakamska, N. L., & Greene, J. E. 2014, MNRAS, 442, 784
Zakamska, N. L., Hamann, F., Pâris, I., et al. 2016, MNRAS, 459, 3144